ORIGINAL PAPER

Seasonal variation of mountain-valley wind circulation and surface layer parameters over the mountainous terrain of the northeastern region of India

Nilamoni Barman[1] · Arup Borgohain[2] · Shyam S. Kundu[2] · N. V. P. Kiran Kumar[3]

Abstract
Mountainous topography and solar elevation angle have a significant influence on the wind circulation and energy exchange over a complex region. Here, the seasonal variation of mountain-valley wind circulation (MVWC) and surface layer parameters have been presented over a hilly station of northeastern India. For the study, quick-response sonic anemometer data have been utilized. The solar elevation angle varies from 85° to 43° in different seasons and controls the MVWC over the terrain. MVWC was dominated in winter (WN), pre-monsoon (PM), and post-monsoon (PMN) seasons, while the synoptic wind predominates the wind direction over the terrain in monsoon (MN). In WN and PM, nighttime heat transmission from the atmosphere to the ground was −10 to −20 W m^{-2}, while the minimum in MN and PMN was −3 to −7 W m^{-2}. The net seasonal daily mean sensible heat flux (H) values from the surface to the atmosphere were 42 W m^{-2}, 58 W m^{-2}, 35 W m^{-2}, and 34 W m^{-2} in WN, PM, MN, and PMN. In MN, the average daytime temperature was 8 °C, 0.5 °C, and 3 °C higher and at night was 9.5 °C, 2 °C, and 4.5 °C higher than the WN, PM, and PMN. In WN, PM, and PMN, the momentum flux had a higher value of about 2 to 3 h after the maximum value in H was attained at the 6-m and 10-m levels. The daytime turbulence kinetic energy was higher by 99%, 56%, 72%, and 93% than the nighttime during WN, PM, MN, and PMN.

1 Introduction

Land-atmosphere interactions that include several processes take place between the earth's surface and the lowermost atmospheric layer. These processes have a substantial impact on the earth's weather and climate systems, energy-budget,

✉ Nilamoni Barman
  neelspinor@gmail.com

  Arup Borgohain
  arupborgohain@gmail.com

  Shyam S. Kundu
  ssk.nesac@gmail.com

  N. V. P. Kiran Kumar
  Kirankumar_nvp@vssc.gov.in

[1] Central Ground Water Board, Eastern Region, Kolkata, West Bengal 700091, India

[2] Space and Atmospheric Science Division, North-Eastern Space Applications Centre, Shillong 793103, India

[3] Space Physics Laboratory, Vikram Sarabhai Space Centre, Trivandrum, India

hydrological cycle, and biogeochemical cycle (Pielke and Avissar 1990; Dickinson 1995). These interactions take place through complicated natural processes (dynamic, physical, biological, and hydrological) and are influenced by terrain, land features, and surface vegetation (Sellers et al. 1995; Barman et al. 2019a, 2019b). Mountain areas display an intense variability in leaf area, ice cover, moisture content, land quality, and rock outcrop that could span a broad variety of lengths from miles to thousands of miles (Wekker et al. 2018). Albedo, terrain-slope, aspect, terrain shading, sky-watch factor, and elevation bring considerable alteration in short- and long-wave solar radiation that causes variability in the available energy which in turn drives the mechanisms of atmospheric exchange. Surface reaching solar insolation as well as in precipitation, soil moisture, and winds affects the air temperature and moisture in microclimates that are essential for studies on meteorology, hydrology, ecology, and agriculture (Wekker et al. 2018). Lehner and Rotach (2018) and Barman et al. (2019b) addressed the evolution and complexities of turbulent transportation and interchange of momentum, heat, and mass in complex terrain. Turbulent flows induced by thermally powered slopes and valley wind may associate with the boundary layer instability at mountains,

resulting in intense vertical transportation of vapor and aerosols (Serafin et al. 2018; Barman et al. 2019b).

Furthermore, surface cover variability and the topography of any high-altitude land have a massive influence on meteorological variables (sensible heat flux (H), momentum flux (τ), turbulence kinetic energy (TKE, e)) (Whiteman 2000; Moraes et al. 2005; Vickers and Mahrt 2006; Bianco et al. 2011; Barman et al. 2019b). Lian-Tong et al. (2010) found that the H changes in the afternoon and nighttime are strikingly different, and the instantaneous flux change in the afternoon is greater than that in the nighttime in northwest China. They also showed that the daytime and seasonal dependency of H variations is highly connected with the daytime variation of mean surface-atmosphere temperature. Solanki et al. (2019) reported that the H shows higher daytime variations in clear sky days over central Himalayas (Nainital), which are in line with the average upward wind velocity. Similarly, in the morning hours, the changes of τ and TKE are less prevalent, when the wind direction shift over the mountain. Srivastava and Sarthi (2002) showed that the monsoons' characteristics are small H and significantly high wind shear, especially in its active period over the eastern region of India. This is because the monsoon season transports a huge amount of water vapor over the area which blocks the solar radiation through the cloud cover and generates a surface-level wind shear owing to the intense wind, which ultimately causes a less H and greater wind shear.

In mountainous regions, the mountain wind circulation has a major effect on zonal climate, weather, ecology, and natural resources (Yang et al. 2016; Jin et al. 2016; Bei et al. 2018; Xu et al. 2018; Li et al. 2019). The wind could be slope wind, valley wind, or mountain-valley wind, with variable wind directions under the weak synoptic influence (Vergeiner and Dreiseitl 1987; Zardi and Whiteman 2012; Tian and Miao 2019; Hernández-Ceballos et al. 2013; Barman et al. 2019a, b). These three wind circulations coexist in diverse mountain ranges such as the Alps and the Pyrenees (Isaksson 2016), Central Himalaya (Solanki et al. 2019), and Meghalaya Plateau (Barman et al. 2019a) and dominate various parts of the mountain. In many other places around the globe, extensive work has been done on the influence of surface conditions and synoptic wind on the mountain wind circulations (Whiteman and Doran 1993; Liu et al. 2004; Wang et al. 2015; Sun et al. 2018). The complicated meteorological processes over the mountainous region affect the dynamic and convective processes in downstream areas (Fernando et al. 2015; Whiteman 2000).

Impacts of topography-induced flow on the surface layer parameters in different seasons still have not been consistently measured under differing weather conditions. It is the first analysis that presents the seasonal variation of surface layer parameters over a mountainous station in the northeastern region of India. The prime objective of this investigation is to enhance the understanding of the mountain-valley wind circulation, seasonal wind pattern, surface layer parameters, and influence of synoptic wind on micrometeorology over the complex terrain, located in between the mountain range of the Himalayan range and the Bay of Bengal.

2 Observational site

The observational station (flux tower) is within the premises of the North-Eastern Space Applications Centre (NESAC), Umiam, Shillong, Meghalaya, India (25.65° N, 91.88° E)—Shillong is the state head quarter of Meghalaya, which is a state in north-east India (Fig. 1). The station is on a plateau at an elevation of approximately 1040 masl and approximately 150 km south from the Himalayan mountain range (altitudes >5000 m). The plateau of Meghalaya overlooks Bangladesh towards the south and Brahmaputra valley to the north. The Shillong peak (Khasi hill's peak) with an altitude of 1961 m is situated at a distance of approximately 20 km from the site towards the south. The site is situated topographically in complex terrain dominated by pine trees, with a large water body (Umiam Lake with a total area of 6.6 km^2) along the south-west direction. The observation tower is installed 900 m away from the lake. Within a radial distance of 1 km from the flux tower, the hills along the east and south-east direction have a slope of approximately 5° to 6°, while the slope along the south-west direction is close to 2°. The tower is located ~100 m above a small valley with a few industrial establishments and is built on grassland with bushes in the nearby area. The elaborated site description is given in Barman et al. (2019a). Mean seasonal rainfall over the observation site is 30 mm, 392 mm, 1416 mm, and 288 mm during the winter (WN), pre-monsoon (PM), monsoon (MN), and post-monsoon (PMN), respectively, as measured by an Automatic Weather Station from 2015 to 2017. It may be mentioned that most of north-east India receives over 80% of its yearly precipitation in the monsoon season.

3 Instrumentation and methodology

3.1 Instrumentation

Four fast-response sonic anemometers (25 Hz) were installed at 6 m, 10 m, 18 m, and 30 m above the surface on a 31-m meteorological tower. The details about the ultrasonic anemometer can be found in Barman et al. (2019a, 2019b) and CSAT3 (2014). The wind data at the 18-m level was not available for analysis as the anemometer was non-functional due to a technical problem. The data from the 6-m, 10-m, and 30-m levels have only been used for analysis here. Three years' data from 1 March 2015 to 31 December 2017 with
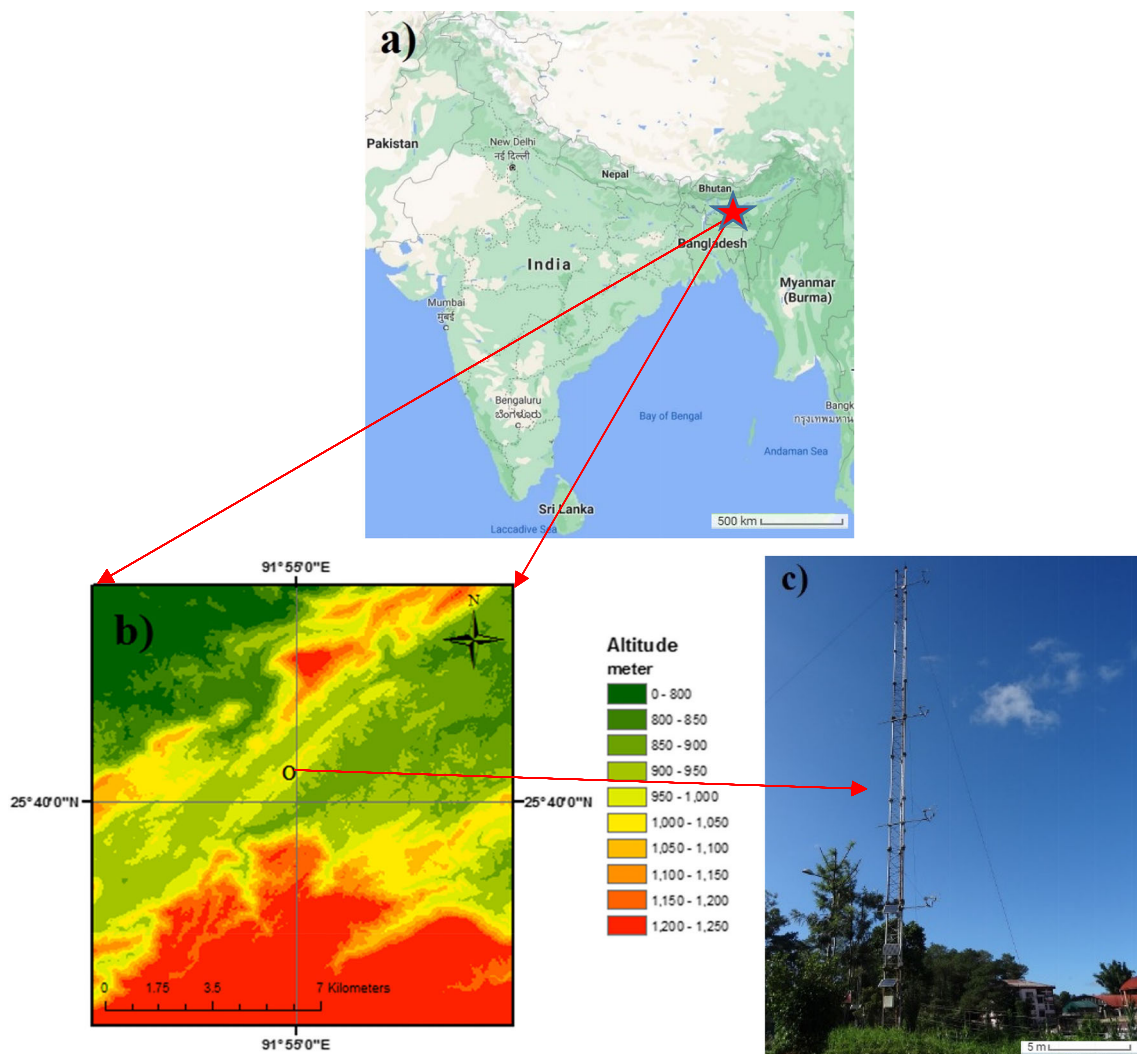
Fig. 1 **a** Google Map of India and observation site (marked by a red star) on the map. **b** High-resolution topographical map of the terrain (the black circle indicates the station) captured from Bhuvan portal (NRSC, ISRO) CARTOSAT-1 digital elevation model (DEM). **c** Image of the instrumented flux tower taken from a distance of 50–60 m in the north-east direction. Adopted from Barman et al. (2019a)

504 cloud-free day observations have been used in the final analysis. Out of 504 clear sky days, 114, 142, 141, and 107 days of data were available from winter (WN—December, January, and February), pre-monsoon (PM—March, April, and May), monsoon (MN—June, July, August, and September), and post-monsoon (PMN—October and November) seasons, respectively. The solar elevation angle at the location is calculated with the help of the NOAA ESRL Solar Position Calculator (https://www.esrl.noaa.gov/gmd/grad/solcalc/azel.html).

3.2 Coordinate rotation

The station located on a mountainous topography and, therefore, before the analysis, flux data were subject to correction (Barman et al. 2019a). Here, the study concentrated on the seasonal variation of surface layer parameters. Hence, data correction and quality checks are not

discussed thoroughly in this study. The detailed data processing and correction conducted were done as per Barman et al. (2019a). The planar fit coordinate rotation technique is utilized to correct the flux dataset. The data from clear sky days only have been considered for the utilization of the planar fit method. In this exercise, multiple linear regression was used to measure the planar fit coefficients or regression coefficients (b_0, b_1, and b_2). Besides, these factors are employed to estimate the pitch (α) and roll (β) angles for tilt correction by adopting the method used by Wilczak et al. (2001). The method defines a hypothetical plane in 3D space where the term b_0 is the plane's intercept, and b_1 and b_2 are partial regression coefficients. The term b_1 specifies the fluctuation in w (vertical wind) when v (meridional wind) is constant for a unit variation in u (zonal wind) and vice versa for b_2. To correct the orthogonal velocity components over a given terrain, the planar fit coefficients along with the roll and

pitch angles are utilized. Only the corrected components are used to calculate the derived surface layer parameters, i.e., H, TKE, τ, and wind speed. For a better understanding of micrometeorology over the study location, we exhibited the daily variation of corrected surface layer parameters.

3.3 Data quality check

The quality analysis of 30-min flux data was carried out by utilizing stationary tests that are employed in the mountainous site (Foken and Wichura 1996; Barman et al. 2019a, 2019b). Non-stationarity is manifested by the alteration of weather parameters, variation in synoptic wind circulation, and a major change in mesoscale wind circulation. The stationarity signifies that the statistics do not differ over time and the lack of stationarity is one of the greatest concerns in turbulence estimation (Foken and Wichura 1996). The stationarity test is used to compare the average flux values with each 30-min duration for the average values with the six respective 5-min sub-durations that constituted the 30 min. Only those fluxes which are measured under the mean wind speed greater than $1~\mathrm{ms}^{-1}$ ($U > 1~\mathrm{m~s}^{-1}$) were considered. The frequency of non-stationary motions indicates a strong correlation with U instead of stability and decreases as mean wind speed increases (Liang et al. 2014).

3.4 Energy and momentum flux

3.4.1 Sensible heat flux

Across the surface of the earth, H plays a critical aspect in the microclimates, and adjacent to the ground, it is impacted by the topography, plants, soils, landforms, and structures (Bonan 2002). The H is expressed as

$$H = \rho C_p \left(\overline{w' \theta_v'} \right) \tag{1}$$

where ρ and C_p are the density of the atmosphere and the isobaric specific heat of air, and w' and θ_v' are the perturbation of w and virtual potential temperature, respectively.

3.4.2 Momentum flux

τ is estimated from the covariance of the horizontal wind (u', v') component's fluctuations and fluctuation of the vertical (w') wind by applying

$$\tau = \rho \sqrt{ \left(\overline{u'w'} \right)^2 + \left(\overline{v'w'} \right)^2 } \tag{2}$$

3.4.3 Turbulence kinetic energy

TKE is directly related to the transportation of momentum, heat, and moisture in the atmospheric boundary layer. Mean TKE is estimated as

$$e = \frac{1}{2} \left(\overline{u'^2} + \overline{v'^2} + \overline{w'^2} \right) \tag{3}$$

4 Results and discussion

4.1 Impact of solar elevation on the regional meteorology

In Fig. 2, the hourly variations of solar elevation angle (φ) for the different seasons have been presented during daytime [0700–1700 LT, local time (LT) = UTC + 05.30 h]. The solar elevation angle is the angular height of the sun in the sky when measured from the horizon. This angle varies between $-10°$ and $90°$. In WN, φ starts from a minimum ($-8°$) in the morning (0700 LT) and reached the maximum (43°) at midday (1200–1300 LT); φ declined to the minimum ($-9°$) in the evening (1900 LT). In PM and MN, φ starts from a minimum of 7° and 10° in the morning (0700 LT) and reaches the maximum of 74° and 85° in the evening (1300 LT); φ declined to a minimum of 2° and 8° in the evening (1900 LT). In PMN, φ starts from a minimum of 2° in the morning (0700 LT) and reached the maximum of 55° at the midday (1200–1300 LT); φ declined to a minimum of $-9°$ in the evening (1900 LT). In all the seasons, the φ reached the maximum at the midday (1200–1300 LT), while a difference of 31°, 42°, and 12° in the elevation angle was observed in the PM, MN, and PMN seasons than the WN season. In WN, as the φ is small, the
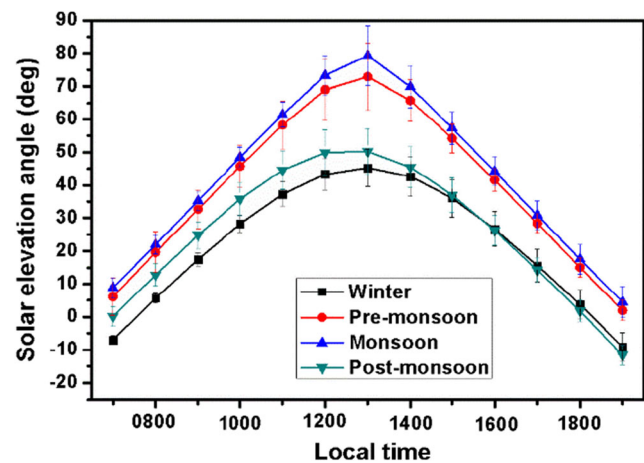

Fig. 2 Seasonal mean diurnal variation (solid line) and standard deviation (vertical bar) of solar elevation angle during winter (in black), pre-monsoon (in red), monsoon (in blue), and post-monsoon (in dark cyan) over the station

surface reaching solar radiation intensity also moderates, and the formation of the cloud is very less. In PM, as φ increased, the evaporation also increased and the evaporation and evapotranspiration also increased from the soil, vegetation, and water body, which contributed to the higher relative humidity (RH) value over the station. In MN, moisture contributed by the local sources (wet soil, vegetation, and water body) along with moisture carried by the south-west monsoon flow accelerates the cloud formation. In PMN, as φ declined, the evaporation and cloud formation activities also reduced. In WN and PM, the average decline of the solar elevation angle in the afternoon was the same, while in PM and MN, the average decline of the solar elevation angle in the morning and afternoon was approximately the same.

4.2 Seasonal wind speed and wind direction

There are three different ways of airmass exchange mechanisms between hilly topography and adjoining dale, e.g., hilly winds, dale wind movement along the plane axis, and larger-scale air circulation between elevated plain and dale (Vergeiner et al. 1987; Zardi and Whiteman 2012; Tian and Miao 2019; Hernandez-Ceballos et al. 2019; Barman et al. 2019a, b). These thermally forced wind circulations

manifested under weak synoptic wind conditions when the ground-level wind circulations are not impacted by the larger-scale synoptic flow. The seasonal diurnal variations of wind speed and direction are presented in Figs. 3 and 4. The wind direction variability represents a mountain-valley wind circulation at the site in WN. Over the site, the prevailing wind direction was from the south-west (200°–330°) sector in the morning, while for the rest of the time, the prevailing wind flow was the south-east (25°–170°) sector (Barman et al. 2019a). In WN, due to dry conditions and moderate wind speeds, more clear days provide a good platform for the evolution of the surface layer parameters and atmospheric boundary layer. During the daytime, a temperature variation between the valley and nearby hilly regions occurs, while at nighttime, surface cooling within the valley produces a localized pressure gradient along the valley, which in turn acts as the only leading force for the circulation. It exhibits a specific periodic rhythm as up-slope flow (up-valley wind) appeared during the day hours and the nighttime experiences downslope flow (down-valley winds). In the PM season, the wind direction was restricted to the south-east (90°–180°) and wind speed also increased at the higher level (30 m) compared to WN. The higher wind speed at the higher level indicated an influence of synoptic flow over the station during the PM
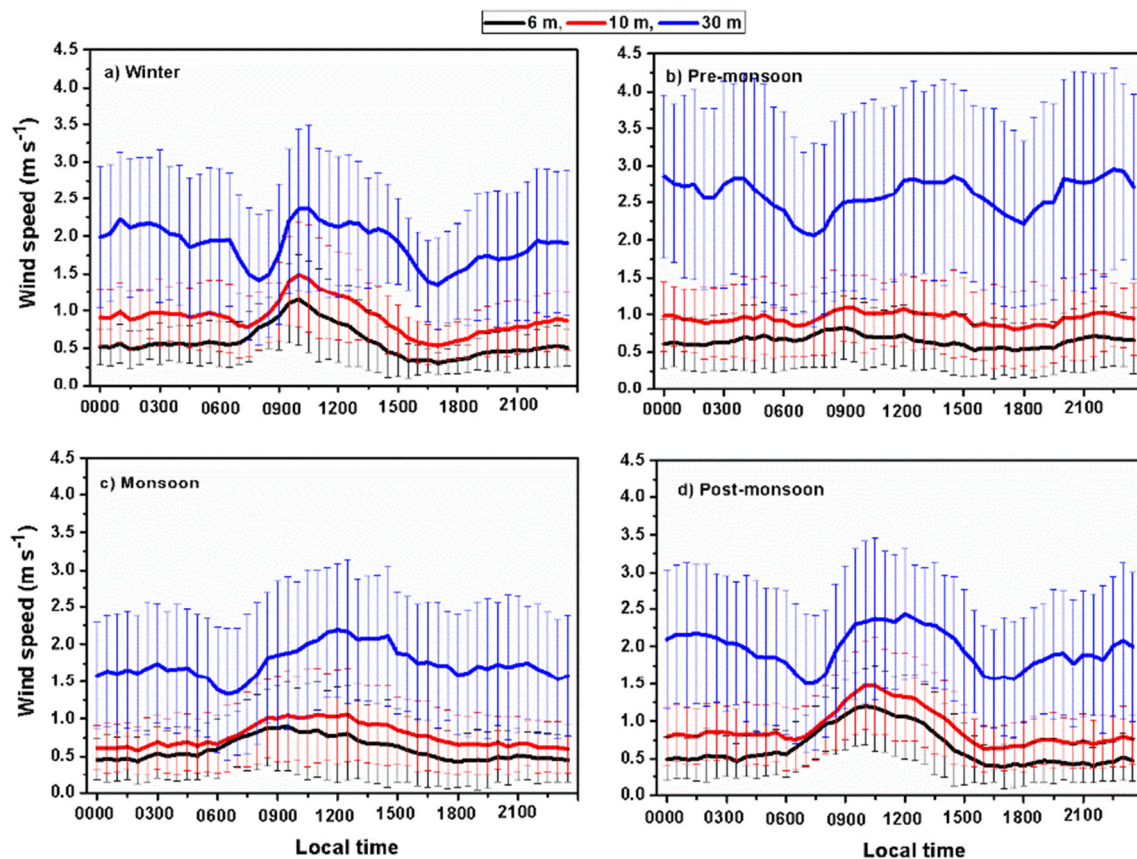

Fig. 3 Seasonal mean daily variation of the mean (line) and standard deviation (vertical bar) of wind speed at the 6-m (in black), 10-m (in red), and 30-m (in blue) heights during **a** winter, **b** pre-monsoon, **c** monsoon, and **d** post-monsoon seasons
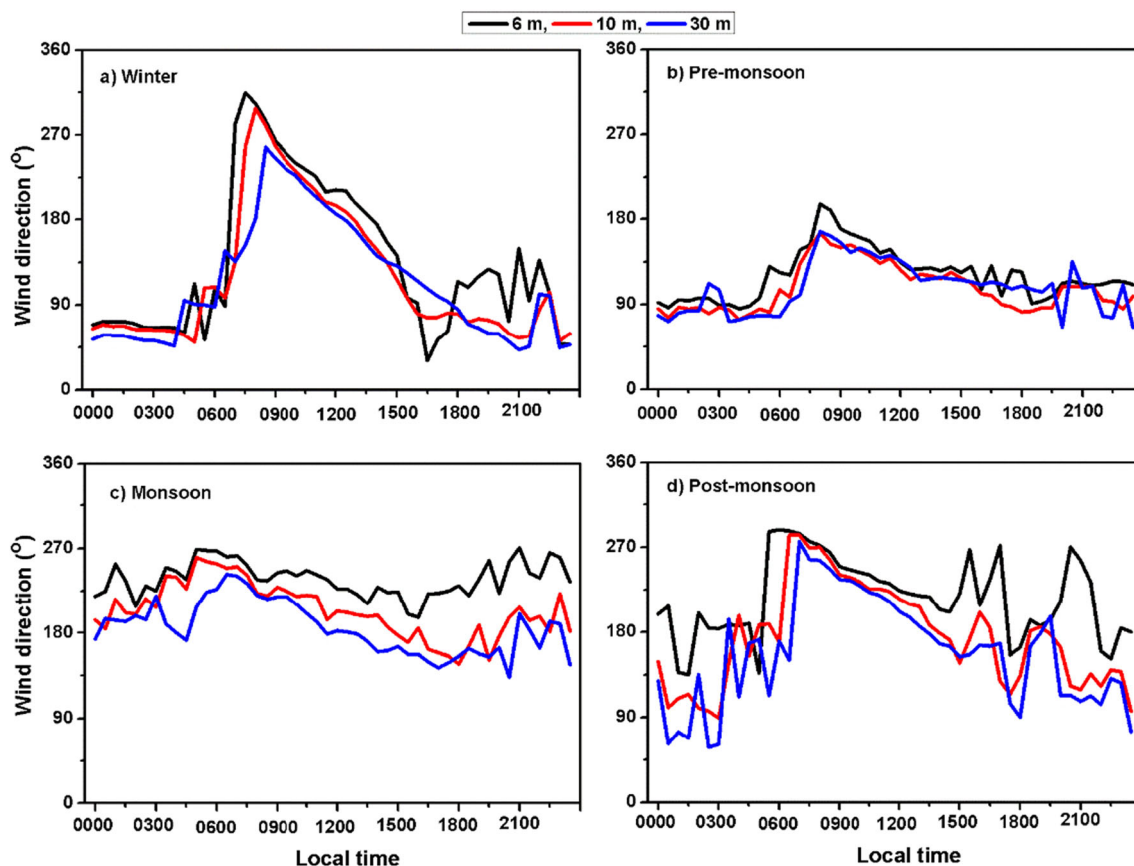
Fig. 4 Seasonal mean daily variation of mean wind direction (solid line) at the 6-m (in black), 10-m (in red), and 30-m (in blue) heights during **a** winter, **b** pre-monsoon, **c** monsoon, and **d** post-monsoon seasons

season. For the synoptic flow, wind vectors at 10-m and 50-m heights from the surface have been presented for detailed study (Fig. S.1 and Fig. S.2, Supplementary Material). Synoptic flow's influence has been visualized in the vector fluxes at a higher level (30 m). In MN, the wind direction was limited to the southward direction (180°–270°) throughout the day. In MN, the mountain-valley wind circulation was suppressed and flow was maintained in a particular sector. In PMN, wind direction varies from the north-east (45°) to west (300°) and mountain-valley wind circulation manifested at the site. Basically, in WN, the sun transits over the site at a smaller elevation angle (43° ± 4°), due to which solar radiation incidents at sun facing the side of the terrain (east) in the morning with the prevailing wind from the south-west direction and in the afternoon, sunshine incident on another side of the hill (west direction) with the prevailing flow from the south-east direction. In PM and MN, sun elevation angles were largest (70° ± 9° and 73° ± 6°), which means that the sun remains for a longer time right over the head. This enables the solar radiation to fall equally over the site during this season and prevailing wind remains from the south-east (90°–180°) and south-west (180°–240°) direction. However, in the PMN season, a smaller sun elevation angle (50° ± 6°) induced mountain-valley wind circulation at the site (Figs. 3 and 4).

4.3 Seasonal variation of relative humidity and temperature

Seasonal mean daily variations in relative humidity (RH) were investigated for WN, PM, MN, and PMN (Fig. 5). In WN and PMN, mean RH values were minimum (56% and 61%) during the daytime and increased to the maximum (88% and 85%) in the nighttime. While in PM, during daytime, RH value was below 47% and increased up to 69% in the nighttime. In MN, due to a higher rate of precipitation, the value of RH was below 73% in the daytime which increased up to 89% in the nighttime. During the nighttime, the RH values rose until midnight to dawn (0000–0600 LT), when the mean RH value was more than 80% and occasionally indeed reached saturation stage. Relative humidity showed a perfect diurnal (0800–1600 LT) variation in all seasons. As the ambient temperature increased due to surface heating during the daytime, RH values decreased. In WN and PM, the nighttime increment of RH value was greater, whereas the minimum values of RH were also observed during these seasons over the site in diurnal hours. The evening rise in the relative humidity occurred owing to the shallow ABL and moisture transported from the south-east direction to the station (Barman et al. 2019a). In MN, the local factor as higher soil moisture, evaporation from the water
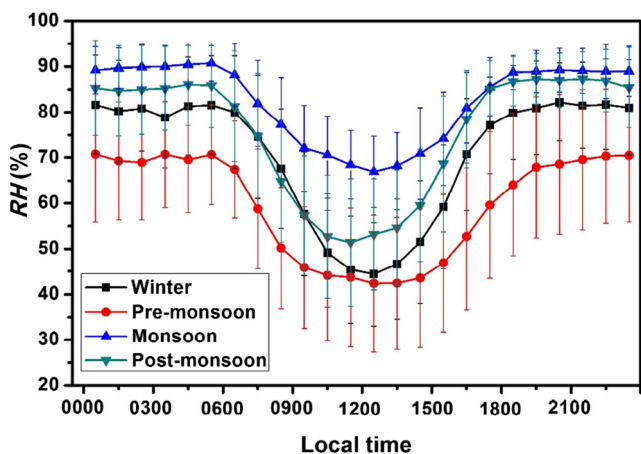
Fig. 5 Seasonal mean daily variation (solid line) and standard deviation (vertical bar) of relative humidity during winter (in black), pre-monsoon (in red), monsoon (in blue), and post-monsoon (in dark cyan) seasons at the station

body, and vegetation enhanced the quantity of water vapor on the local scale, and simultaneously, south-west monsoon also added a higher quantity of moisture over the terrain. In PMN, the enhancement of RH value solely depended on the local factors. Water vapor contributes significantly to the greenhouse effect, and RH typically remains between 35 and 65% for clear sky conditions and between 65 and 85% for cloudy days (Wei et al. 2019). Gordon et al. (2013) showed the short-term warming effect of water vapor is 2.2 ± 0.4 W m^{-2} K^{-1} and also estimated a range of likely values for the long-term twentieth century water vapor feedback at 1.9 to 2.8 W m^{-2} K^{-1}. The seasonal mean daily variation of mixing ratio was most prominent and varies between 7.3 ± 0.6 and 15 ± 0.7 g kg^{-1} in different seasons. In WN and PM, the mean mixing ratio was lowest (7.3 and 9.7 g kg^{-1}) and highest in MN and PMN (15 g kg^{-1} and 11 g kg^{-1}). In the morning hours, the evapo-transpiration of surface water (dew, soil water, and plant water) added moisture (by flux convergence) to the lower layers and the humidity increased quite sharply into a moderately unstable atmosphere (Fig. 5). By early afternoon, the peak humidity concentration dropped slightly. In the late afternoon, surface cooling was strong and the lowest layers became stable. Thus, the ability to transport vapor to the higher layer was less than the rate at which it continued to be added from the surface. Moisture converges into the lowest layers and a second humidity maximum is observed. Thereafter, evapotranspiration declined in the nighttime.

Figure 6 illustrates the diurnal cycle of air temperature at different heights. The profile of air temperature shows maxima at the height where the mean leaf area peaks. This is the
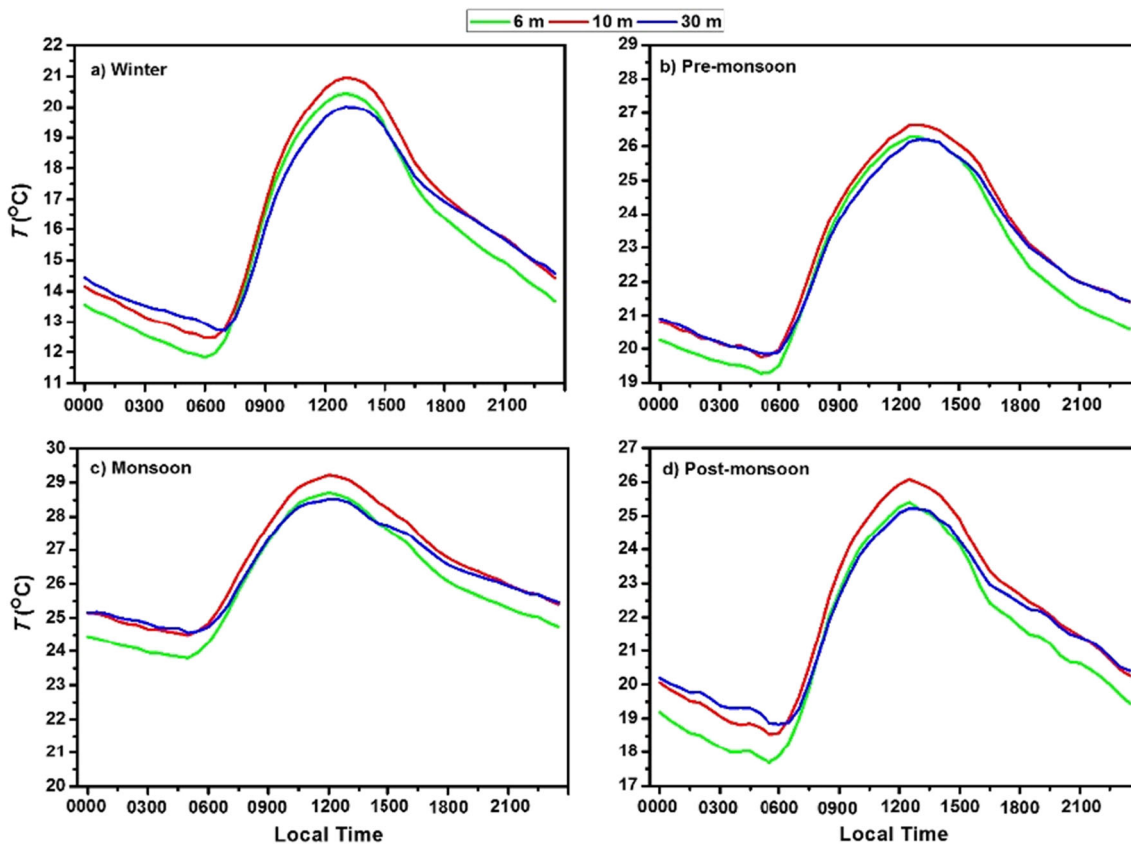

Fig. 6 Seasonal mean daily temperature variation (solid line) during **a** winter, **b** pre-monsoon, **c** monsoon, and **d** post-monsoon seasons at 6 m (in green), 10 m (in red), and 30 m (in blue) at the station

height where the absorption and transpiration of incoming radiation produced higher heat and moisture. As the station is surrounded by plants (dominantly by the Khasi pine plants with an average height approximately 8–10 m), the daytime air temperature was higher at the 10-m level in all the seasons. There is a temperature inversion under different seasons during the nighttime the leaf canopy since the leaf canopy is warmer than the floor where only weak radiative absorption (Oke 1987). Within the soil, there is usually very little temperature variation with depth or time (Abu-Hamdeh 2003). The humidity profile is difficult to generalize within the stand because of the possibility of soil evaporation, or plants on the floor. The temperature profile is reversed at the night with a minimal in the leaf canopy's upper part, an inversion above, and lapse below (Oke 1987). The reduced sky view factor for places below the canopy eliminates long-wave radiative losses and helps to preserve relatively mild situations within the stand compared with those in the open or above the trees. During a fine weather day, surface evaporative cooling promotes a surface-based inversion. Since the moist cool surface is overlaid by hot air, the "oasis-effect" is followed by an inversion (Oke 1987). Via evaporation, summer rain can also cool the surface and lead to a similar temperature profile.

In Fig. 7, we have shown the temperature inversion (TI) for different seasons during the nighttime (1900–0500 LT) over the station. TI is an important feature of the atmospheric boundary layer. It reduces or even stops the vertical exchange between the atmospheric boundary layer air below the inversion and the air above it. It is particularly relevant for the turbulent vertical exchange of heat, momentum, water vapor, and other constituents. Here, TI ($TI_{10m–6m}$, $TI_{30m–6m}$) was investigated at the 6-m, 10-m, and 30-m levels at the site. The mean seasonal TI values between 10 m (30 m) and 6 m were 0.68 °C (0.19 °C), 0.64 °C (0.02 °C), 0.7 °C (0.04 °C), and 0.87 °C (0.18 °C) in the WN, PM, MN, and PMN seasons, respectively. $TI_{10m–6m}$ was higher in WN than in PM and increased from PM to PMN, while $TI_{30m–6m}$ increased from PM to PMN. In WN, as the mountain-valley wind circulation

dominated over the site, the moist air was transported through the valley axis to the cooler surface of the station.

4.4 Diurnal temperature range

Diurnal temperature range (DTR), defined as the difference between daily maxima (T_{max}) and minima (T_{min}) temperatures, is a key driving factor in most of the climatological processes (Dai et al. 1999; Rai et al. 2012; Davy et al. 2016) and is an important index of diurnal variations (Cook 2016). In general, over the station, the daytime average temperature was 6 °C, 6 °C, 4.5 °C, and 6 °C higher than the nighttime average temperature in WN, PM, MN, and PMN, respectively. In the monsoon season, the daytime average temperature was 8 °C, 0.5 °C, and 3 °C higher than the WN, PM, and PMN, respectively. Similarly, the nighttime average temperature in the MN season was 9.5 °C, 2 °C, and 4.5 °C higher than the WN, PM, and PMN, respectively. Donat et al. (2013), Miao et al. (2016), and Shrestha et al. (2016) reported that the intensity, frequency, and duration of extreme precipitation events increase, with a less difference between daytime and nighttime temperatures, when the same is because of enhancement in nighttime temperatures than daytime temperatures. In MN, we observed that the average temperature variation between day and night was lesser than the other seasons, which is perhaps one of the explanations for the higher rainfall over the terrain. The uptick in cloud cover appears to reduce T_{max}, although its overall effect on T_{min} has comparatively less reflectivity of the clouds that lower midday temperatures and therefore T_{min}, while it also boosts downward long-wave radiation that improves T_{min} and allows DTR to drop. The higher rainfall also leads to decreasing DTR through the cooling of surface evaporation (Dai et al. 1999). Solar heating is balanced by evapotranspiration, coupled with the moisture of soil, and rainfall causes a decrease in T_{max} (Dai et al. 1999). Furthermore, the atmospheric impact on water vapor on DTR is insignificant since its effect on T_{max} and T_{min} is comparable (Dai et al. 1999).
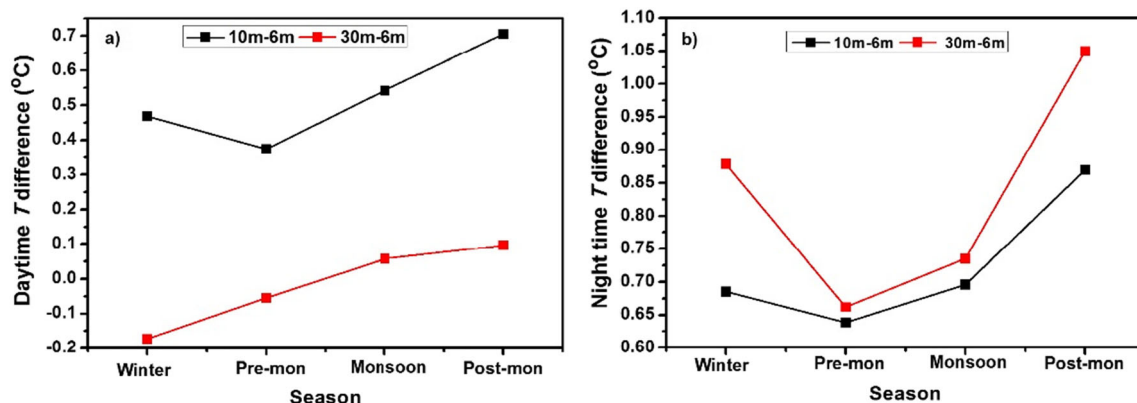

Fig. 7 The seasonal **a** mean daytime and **b** mean nighttime temperature difference between 10 and 6 m (in black) and between 30 and 6 m (in red) at the station

4.5 Influence of synoptic flow

In Figs. S.1 and S.2 (Online resource), the seasonal mean wind vector plots at 10 m and 50 m above the surface level have been used to represent the influence of synoptic flow over the station. In the WN and PMN seasons, the westerly flow dominated over the study region. As soon as the westerly flow reaches northeast India, it is divided into two streams, one flowing along the northeast direction and the second stream continues in the east direction. The sidewalls of Brahmaputra valley, i.e., the hills in Bhutan and Meghalaya, have an impact on the westerly flow and cause the flow separation in different directions (Figs. S.1a, d, and S.2a, d). However, in PM and MN seasons, south westerly synoptic flow dominated over the region. South-west flow moves along the Bay of Bengal and crosses Bangladesh without any disturbance, but as soon as the flow reaches the Meghalaya Plateau, it gets bifurcated of the flow along northward and north-eastward direction. The Shillong peak plays a vital role in the flow separation in the PM and MN seasons. The wind velocity in WN and PMN is lower compared to that in PM and MN seasons at the surface level (10 m and 50 m) (Fig. S.2b, c).

5 Seasonal surface flux variation

The fast-response sonic anemometer has been used to estimate the diurnal variation of seasonal mean TKE, τ, and H at 6-m, 10-m, and 30-m heights during WN, PM, MN, and PMN seasons around the Umiam (Figs. S.3, S.4, and S.5 (Online resource)).

5.1 Turbulence kinetic energy

Turbulence is produced thermally through buoyancy effects (daytime heat-driven mesoscale circulations) and mechanically through shear (nighttime low-level jets and mountain waves) in complex terrain (Serafin et al. 2018; Adler and Kalthoff 2016). Surface-level turbulence plays a major role in transporting energy and pollutants. Hence, this section explains the effect of the mountain-valley wind circulation on the turbulence feature and turbulent fluxes over the location.

The seasonal mean daytime variation of TKE showed a distinct pattern in WN, PM, MN, and PMN at 6-m, 10-m, and 30-m levels at the station, respectively (Fig. S.3). Barman et al. (2019b) demonstrated that the mountain-valley wind circulation has an effect on the surface-level turbulence or TKE at the station. In the daytime, TKE values at higher height (30-m level) were higher (59%, 71%, 51%, and 41%) than those at the lower height (6-m level) in WN, PM, MN, and PMN, respectively. The higher TKE value in PM season can be associated with the higher wind speed at the higher level (30 m). In PM, the synoptic flow has an impact over the station, which could be visualized in the TKE values. The daytime TKE values were higher (99%, 56%, 72%, and 93%) than the nighttime values in WN, PM, MN, and PMN, respectively. In PM, the lower difference in day-night values of TKE indicates the influence of synoptic flow at a higher level. In the WN season, two peak values of TKE were found in the morning and afternoon periods. The transition of TKE's short time transition at 1200–1300 LT is linked with a fast change in ground-level wind speed gradients and fluxes, which is predominated over the westerly synoptic flow. The morning peak (MP) was higher than the afternoon peak (AP) at the 6-m level, whereas, MP and AP were almost equal at the 10-m height. On the other hand, the AP was higher than the MP at the 30-m level. In the PM season, the TKE peak value occurred in the afternoon at all the levels. In MN, TKE is higher at 30-m height which indicated a higher rate of air mixing between the 10-m and 30-m layer of the atmosphere. TKE and H reached their peak almost simultaneously in all the seasons. The turbulence rate in the stable atmosphere enhances from nil to the height of the convective boundary layer, known as the spin-up process (Stull 1988). Owing to reduced wind speed and solar radiation, TKE values declined with time in the noontime. TKE decline with time in the noon hours known as the spin-down process occurs owing to the dissipation and loss of excess turbulence generation (Stull 1988). Daily TKE variability indicated an increase in turbulence severity in diurnal hours and decrease at the nocturnal hours. The TKE exhibits a linear increment in turbulence generation, leading to greater diurnal land heating and faster wind condition. Intriguingly, the nighttime TKE values also enhanced from WN to PMN that implied a higher turbulence intensity because of higher wind speeds. TKEs on the short-term transition between 1200 and 1300 LT is correlated with a dramatic change in surface wind speed gradients and fluxes in the WN, PM, and PMN seasons.

5.2 Momentum flux

The momentum flux (τ) showed a distinct diurnal variation throughout all the seasons, as displayed in Fig. S.4. Barman et al. (2019b) demonstrated that the wind speed over the site increased by midday and produced a higher τ and TKE at the station in the WN season, with two peaks of τ observed in the morning and afternoon periods. The MP was higher than the AP at the 6-m level. While at the 10-m height, MP and AP were almost equal. On the other hand, at the 30-m level, the AP was higher than the MP (Fig. S.4a). In the PM season, the MP was higher than the AP at the 6-m level. However, the AP was higher than the MP at the 10-m and 30-m levels (Fig. S.4b). In the MN season, peak value was observed in the afternoon. In the WN, PM, and PMN seasons, the τ attained a higher value at about 2 to 3 h after the maximum value in H at the 6-m and 10-m levels, while in the MN season, the peak τ value occurred along with the peak H values. τ is correlated to

the covariance of velocity perturbation, and thus the higher wind speed at higher height during the PM season contributed to higher τ values at all levels. Due to the variation in wind direction from the south-west to the south-east in the day hours in WN, PM, and PMN, the τ value dropped at 1130–1230 LT. It has been observed that a local thermal circulation was prevalent during daytime (Figs. 4a, b, and d), and the wind direction was unpredictable over the day. This wind direction fluctuation played a vital role in the evolution of the surface layer parameters and ABL characteristics over the experimental site.

5.3 Sensible heat flux

The water vapor exchange between the land and the atmosphere influences the relative humidity; like, the sensible heat flux predominantly controls the air temperature in the lowest layers. Moreover, heat is supplied into the air during the daytime which returns to the ground during the nighttime keeping the vapor flux strongly upward (Oke 1987). The daytime variation of H was significant in the WN and PMN seasons, increased systematically in the morning (0730 LT), reached the maximum during 1000–1100 LT, and decreased to minimum values in the afternoon (1530 LT) (Fig. S.5 a, d). In PM, H increased from morning (0630 LT), attained peak value during 1000–1100 LT, and decreased to minimum values in the late afternoon (1630 LT). In the MN season, H increased from morning (0600 LT), reached maximum values during 1100–1200 LT, and decreased to a minimum in the late afternoon (1700 LT). The time of occurrence of the maximum H value was 1–2 h before the highest solar elevation angle over the station. The peak values of H were 219 ± 61 W m^{-2}, 278 ± 120 W m^{-2}, 152 ± 127 W m^{-2}, and 166 ± 68 W m^{-2} in WN (1000–1100 LT), PM (1000–1100 LT), MN (1100–1200 LT), and PMN (1000–1100 LT) respectively at the higher (30 m) height. The peak value of H during PM was the largest while the least value was seen during MN. Such high values of H over the complex terrain during PM are contributed by the higher solar insolation due to the larger solar elevation angle and the intense convective vertical motions that dominated during the daytime. In the WN and PMN seasons, the initiation of the rising of H value was delayed by 30 min to 1 h at the 30-m height in the morning (Figs. S.5a, b, & d), while in the MN season, H value increased equally at all levels (Fig. S.5c). Over the station, as the solar radiation incident on the ground with low elevation angle in the WN and PMN seasons, this caused slow surface heating and delay of H value at 30-m levels. While, in the PM and MN seasons, due to the larger sun elevation angle, the intensity of incident radiation is higher and heats the surface early than the WN and PMN seasons. When the wind direction changed from south-west to south, the value of H decreased at 1130 LT, followed by a slight rise in H before a further decline, and mountain-valley wind circulation is

dominated over westerly synoptic flow. Barman et al. (2019b) demonstrated that the wind direction variability has a significant impact on surface layer parameters, whereas local thermal circulations were found to influence the development of surface layer parameters at the station.

The variation in temperature between the atmosphere and surface leads to the downward thermal energy transition from the ambient to the land at the nighttime. The higher downward heat transfer occurs for the higher temperature difference between the atmosphere and surface. Here, the small downward transfer of heat is measured in the nighttime (typically H from -3 to -20 W m^{-2}). The nighttime H is larger in WN and PM (-10 to -20 W m^{-2}) and least in MN and PMN (typically -3 to -7 W m^{-2}). The negative H was largest in PM (-20 ± 9 W m^{-2}) and smallest in MN (-3 ± 2 W m^{-2}) at the site. The downward heat transfer was higher in WN and PM, while lower in MN and PMN, respectively. Generally, the nighttime air layer above the surface was warmer and maximum downward heat is transferred to the land. However, in MN, the surface contains higher moisture than other seasons and more evaporation is caused by a significant amount of insolation. In the MN, vegetation growth is very high owing to the higher precipitation than the dry season. As the moist soil has a higher specific heat capacity compared to dry soil, the land surface was warmer in the MN season than the PM season. The soil heat capacity is influenced by the soil moisture content and soil density (De Vries 1952; Wierenga et al. 1969). Abu-Hamdeh (2003) further showed that specific heat increases with increasing moisture contained in the soil. Soil management influences soil heat capacity because processes that lead to soil compaction will enhance the total density and decrease the soil porosity, which have a significant effect on heat capacity. The net seasonal diurnal mean H values from the land to the ambient were 42 W m^{-2}, 58 W m^{-2}, 35 W m^{-2}, and 34 W m^{-2} in WN, PM, MN, and PMN, respectively.

6 Conclusions

In the present work, an effort has been made to explain the surface and atmosphere energy exchange over complex terrain in various seasons. In the winter and post-monsoon seasons, mountain-valley circulation (local) dominated over westerly synoptic flow, while in the monsoon and pre-monsoon seasons, south-westerly synoptic dominated over the mountain-valley wind circulation.

In winter, as the solar elevation angle is small, the insolation also moderates over the topography, and cloud development is negligible. A larger solar elevation angle in pre-monsoon increased the evaporation from the soil, vegetation, and water body, which enhanced the higher relative humidity over the terrain. In monsoon, moisture in the atmosphere is strengthened by the contribution from the local sources (wet

soil, vegetation, and water body), and the south-west synoptic circulation transported water vapor into the atmosphere, which advanced the cloud development. In post-monsoon, as the solar elevation angle decreased, the evaporation and cloud formation process further weakened. As the station is surrounded by vegetation, the daytime air temperature was greater at a particular height over the seasons. In winter and post-monsoon, the wind speed is lower in comparison to pre-monsoon and monsoon at the ground level.

In winter and pre-monsoon seasons, the downward heat transfer was greater than that of the other periods. The night-time air layer well above land was warmer and maximum downward heat transferred to the land. While, in monsoon, as the water content in the ground was larger than the other seasons with enhanced insolation, the evaporation process was accelerated. The vegetative surface also enhanced evapo-transpiration. The vegetation growth is significantly high in monsoon because of the greater rainfall amount than the dry seasons. As the wet soil has a greater specific heat capacity than dry soil, the ground is hotter in monsoon compared to the pre-monsoon season. The net seasonal daily mean sensible heat flux from the surface to the atmosphere was higher in pre-monsoon. During the winter, pre-monsoon, and post-monsoon, the momentum flux had a higher value of about 2 to 3 h after the maximum value in the sensible heat flux was attained at the lower height. The difference in day and night turbulence kinetic energy was higher in winter.

Compliance with ethical standards

References

Abu-Hamdeh NH (2003) Thermal properties of soils as affected by density and water content. Biosyst Eng 86(1):97–102. https://doi.org/10.1016/S1537-5110(03)00112-0

Adler B, Kalthoff N (2016) The impact of upstream flow on the atmospheric boundary layer in a valley on a mountainous island. Bound-Layer Meteorol 158:429–452

Barman N, Borgohain A, Kundu SS, Saha B, Roy R, Solanki R, Kiran Kumar NVP, Raju PLN (2019a) Impact of atmospheric conditions in surface–air exchange of energy in a topographically complex terrain over Umiam. Meteorog Atmos Phys. https://doi.org/10.1007/s00703-019-00668-7

Barman N, Borgohain A, Kundu SS, Saha B, Roy R, Solanki R, Kiran Kumar NVP, Raju PLN (2019b) Daytime temporal variation of surface-layer parameters and turbulence kinetic energy budget in topographically complex terrain around Umiam, India. Boundary-Layer Meteorol. https://doi.org/10.1007/s10546-019-00443-6

Bei NF, Zhao LN, Wu JR, Li X, Feng T, Li GH (2018) Impacts of sea-land and mountain-valley circulations on the air pollution in Beijing-Tianjin-Hebei (BTH): a case study. Environ Pollut 234:429–438

Bianco L, Djalalova IV, King CW, Wilczak JM (2011) Diurnal evolution and annual variability of boundary-layer height and its correlation with other meteorological variables in California's Central Valley. Boundary-Layer Meteorol 140:491–511. https://doi.org/10.1007/s10546-011-9622-4

Bonan GB (2002) Ecological climatology. Cambridge University Press, UK

Cook T (2016) Toward a reassessment of daily temperature range trends. Eos (Washington. DC). 97

CSAT3 (2014) Instruction manual: CSAT3 three-dimensional sonic anemometer, Campbell Scientific. Inc

Dai A, Trenberth KE, Karl TR (1999) Effects of clouds, soil moisture, precipitation, and water vapour on diurnal temperature range. J Clim 12:2451–2473

Davy R, Esau I, Chernokulsky A, Outten S, Zilitinkevich S (2016) Diurnal asymmetry to the observed global warming. Int J Climatol. https://doi.org/10.1002/joc.4688

De Vries DA (1952) The thermal conductivity of soil. Meded. Landbouwhogesch, Wageningen, pp 52

Dickinson RE (1995) Land-atmosphere interaction. Rev Geophys Suppl 33:917–922

Donat MG, Alexander LV, Yang H, Durre I, Vose R, Dunn RJH, Willett KM, Aguilar E, Brunet M, Caesar J, Hewitson B, Jack C, Klein Tank AMG, Kruger AC, Marengo J, Peterson TC, Renom M, Oria Rojas C, Rusticucci M, Salinger J, Elrayah AS, Sekele SS, Srivastava AK, Trewin B, Villarroel C, Vincent LA, Zhai P, Zhang X, Kitching (2013) Updated analyses of temperature and precipitation extreme indices since the beginning of the twentieth century: the HadEX2 dataset. J Geophys Res Atmos 118:2098–2118

Fernando HJS, Pardyjak ER, di Sabatino S, Chow FK, de Wekker SFJ, Hoch SW et al (2015) The MATERHORN: unravelling the intricacies of mountain weather. Bulletin of American Meteorological Society 96(11):1945–1967

Foken T, Wichura B (1996) Tools for quality assessment of surface-based flux measurements. Agric For Meteorol 78(1–2):83–105

Gordon ND, Jonko AK, Forster PM, Shell KM (2013) An observationally based constraint on the water-vapor feedback, J Geophys Res Atmos. https://doi.org/10.1002/2013JD020184

Hernández-Ceballos MA, Adame JA, Bolívar JP, De la Morena BA (2013) A mesoscale simulation of coastal circulation in the Guadalquivir valley (southwestern Iberian Peninsula) using the WRF-ARW model. Atmos Res 124:1–20

Isaksson R (2016) Numerical simulation of diurnal planetary boundary layer effects and diurnal mountain-wind effects. Ph.D. Thesis, Uppsala University, Uppsala, Sweden

Jin LL, Li ZJ, He Q, Miao QL, Zhang HQ, Yang XH (2016) Observation and simulation of near-surface wind and its variation with topography in Urumqi, West China. J Meteorol Res 30:961–982

Lehner M, Rotach MW (2018) Current challenges in understanding and predicting transport and exchange in the atmosphere over mountainous terrain. Atmosphere 9:276

Li LL, Li J, Chen HM, Yu RC (2019) Diurnal variations of summer precipitation over the Qilian mountains in Northwest China. J Meteorol Res 33:18–30

Liang J, Zhang L, Wang Y, Cao X, Zhang Q, Wang H, Zhang B (2014) Turbulence regimes and the validity of similarity theory in the stable boundary layer over the complex terrain of the loess plateau. China J Geophys Res Atmos. https://doi.org/10.1002/2014JD021510

Lian-Tong Z, Ren-Guang W, Rong-Hui H (2010) Variability of surface sensible heat flux over Northwest China. Atmospheric and Oceanic Science Letters 3(2):75–80. https://doi.org/10.1080/16742834.2010.11446847

Liu H, Liang B, Zhu FR, Zhang BY, Sang JG (2004) Water-tank experiment on the thermal circulation induced by the bottom heating in an asymmetric valley. Adv Atmos Sci 21:536–546

Miao C, Sun Q, Borthwick AGL, Duan Q (2016) Linkage between hourly precipitation events and atmospheric temperature changes over China during the warm season. Sci Rep 6:22543

Moraes OLL, Acevedo OC, Degrazia GA, Anfossi D, da Silva R, Anabor V (2005) Surface layer turbulence parameters over a complex terrain. Atmos Environ 39:3103–3112

Oke TR (1987) Boundary layer climate. Routledge, Taylor & Francis Group ISBN 0–203–71545-4

Pielke RA, Avissar R (1990) Influence of landscape structure on local and regional climate. Landsc Ecol 4:133–155

Rai A, Joshi MK, Pandey AC (2012) Variations in diurnal temperature range over India: under the global warming scenario. J Geophys Res-Atmos 117:1–12

Sellers PJ, Heiser MD, Hall FG, Goetz SJ, Strebel DE, Verma SB, Desjardins RL, Schuepp PM, MacPherson JI (1995) Effects of spatial variability in topography, vegetation cover and soil moisture on area-averaged surface fluxes: a case study using the FIFE 1989 data. J Geophys Res 100:25

Serafin S, Adler B, Cuxart J, De Wekker SFJ, Gohm A, Grisogono B, Kalthoff N, Kirshbaum DJ, Rotach MW, Schmidli J et al (2018) Exchange processes in the atmospheric boundary layer over mountainous terrain. Atmosphere 9:102

Shrestha AB, Bajracharya SR, Sharma AR, Duo C, Kulkarni A (2016) Observed trends and changes in daily temperature and precipitation extremes over the Koshi river basin 1975–2010. Int J Climatol. https://doi.org/10.1002/joc.4761

Solanki R, Singh N, Kiran Kumar NVP, Rajeev K, Imasu R, Dhaka SK (2019) Impact of mountainous topography on surface-layer parameters during weak mean-flow conditions. Bound-Layer Meteorol. https://doi.org/10.1007/s10546-019-00438-3

Srivastava MK, Sarthi PP (2002) Turbulent kinetic energy in the atmospheric surface layer during the summer monsoon. Meteorol Appl 9:239–246. https://doi.org/10.1017/S1350482702002098

Stull RB (1988) An introduction to boundary layer meteorology. Kluwer Academic Publishers, Dordrecht

Sun FL, Ma YM, Hu ZY, Li MS, Tartari G, Salerno F, Gerken T, Bonasoni P, Cristofanelli P, Vuillermoz E (2018) Mechanism of daytime strong winds on the northern slopes of Himalayas, near Mount Everest: observation and simulation. J Appl Meteorol Climatol 57:255–272

Tian Y, Miao JF (2019) An overview of mountain-valley breeze studies in China. Meteorol Sci Technol 47:41–51

Vergeiner I, Dreiseitl E (1987) Valley winds and slope winds—observations and elementary thoughts. Meteorog Atmos Phys 36:264–286

Vickers D, Mahrt L (2006) A solution for flux contamination by mesoscale motions with very weak turbulence. Boundary-Layer Meteorol 118:431–447

Wang D, Miao JF, Zhang DL (2015) Numerical simulations of local circulation and its response to land cover changes over the Yellow Mountains of China. J Meteorol Res 29:667–681

Wei PS, Chiu HH, Hsieh YC, Yen DL, Lee C, Tsai YC, Ting TC (2019) Absorption coefficient of water vapor across the atmospheric troposphere layer, Heliyon. https://doi.org/10.1016/j.heliyon.2019.e01145

Wekker SFJD, Kossmann M, Knievel JC, Giovannini L, Gutmann ED, Zardi D (2018) Meteorological applications benefiting from an improved understanding of atmospheric exchange processes over mountains, MDPI. Atmosphere 9:371. https://doi.org/10.3390/atmos9100371

Whiteman CD (2000) Mountain meteorology: fundamentals and applications. Oxford University Press; 2000

Whiteman CD, Doran JC (1993) The relationship between overlying synoptic-scale flows and winds within a valley. J Appl Meteorol 32:1669–1682

Wierenga PJ, Nielsen DR, Hagan RM (1969) Thermal properties of soil-based upon field and laboratory measurements. Soil Sci Soc Am Proc 33:354–360

Wilczak JM, Oncley SP, Stage S (2001) Sonic anemometer tilts correction algorithms. Bound-Layer Meteorol 99:127–150

Xu JZ, Assenova A, Erokhin V (2018) Renewable energy and sustainable development in a resource-abundant country: challenges of wind power generation in Kazakhstan. Sustainability 10:3315

Yang Y, Fan JW, Leung LR, Zhao C, Li ZQ, Rosenfeld D (2016) Mechanisms contributing to suppressed precipitation in Mt. Hua of Central China. Part I: mountain valley circulation. J Atmos Sci 73:1351–1366

Zardi D, Whiteman CD (2012) Diurnal mountain wind systems, chapter 2 in mountain weather research and forecasting. Springer, New York, pp 35–119